AGU PUBLICATIONS

JGR

Journal of Geophysical Research: Solid Earth

RESEARCH ARTICLE
10.1002/2017JB014460

Key Points:
- Seismicity spans nearly 10 years with maximum magnitude increasing with time
- Wastewater disposal at five wells has led to an overpressured formation that is hydraulically connected with the seismogenic basement
- Induced earthquakes occur only where the host fault is optimally oriented for failure within the regional stress field

Supporting Information:
- Supporting Information S1
- Data Set S1
- Data Set S2
- Data Set S3
- Data Set S4
- Data Set S5

Correspondence to:
H. R. DeShon,
hdeshon@smu.edu

Citation:
Scales, M. M., DeShon, H. R., Magnani, M. B., Walter, J. I., Quinones, L., Pratt, T. L., & Hornbach, M. J. (2017). A decade of induced slip on the causative fault of the 2015 M_w 4.0 Venus earthquake, northeast Johnson County, Texas. *Journal of Geophysical Research: Solid Earth*, *122*. https://doi.org/10.1002/2017JB014460

Received 22 MAY 2017
Accepted 31 AUG 2017
Accepted article online 4 SEP 2017

A Decade of Induced Slip on the Causative Fault of the 2015 M_w 4.0 Venus Earthquake, Northeast Johnson County, Texas

Monique M. Scales[1], Heather R. DeShon[1], M. Beatrice Magnani[1], Jacob I. Walter[2,3], Louis Quinones[1], Thomas L. Pratt[4], and Matthew J. Hornbach[1]

[1]Roy M. Huffington Department of Earth Sciences, Southern Methodist University, Dallas, TX, USA, [2]Institute for Geophysics, University of Texas at Austin, Austin, TX, USA, [3]Now at Oklahoma Geological Survey, Norman, OK, USA, [4]U.S. Geological Survey, Reston, VA, USA

Abstract On 7 May 2015, a M_w 4.0 earthquake occurred near Venus, northeast Johnson County, Texas, in an area of the Bend Arch-Fort Worth Basin that reports long-term, high-volume wastewater disposal and that has hosted felt earthquakes since 2009. In the weeks following the M_w 4.0 earthquake, we deployed a local seismic network and purchased nearby active-source seismic reflection data to capture additional events, characterize the causative fault, and explore potential links between ongoing industry activity and seismicity. Hypocenter relocations of the resulting local earthquake catalog span ~4–6 km depth and indicate a fault striking ~230°, dipping to the west, consistent with a nodal plane of the M_w 4.0 regional moment tensor. Fault plane solutions indicate normal faulting, with B axes striking parallel to maximum horizontal compressive stress. Seismic reflection data image the reactivated basement fault penetrating the Ordovician disposal layer and Mississippian production layer, but not displacing post-Lower Pennsylvanian units. Template matching at regional seismic stations indicates that low-magnitude earthquakes with similar waveforms began in April 2008, with increasing magnitude over time. Pressure data from five saltwater disposal wells within 5 km of the active fault indicate a disposal formation that is 0.9–4.8 MPa above hydrostatic. We suggest that the injection of 28,000,000 m^3 of wastewater between 2006 and 2015 at these wells led to an increase in subsurface pore fluid pressure that contributed to inducing this long-lived earthquake sequence. The 2015 M_w 4.0 event represents the largest event in the continuing evolution of slip on the causative fault.

1. Introduction

Increasing seismicity rates in the central United States since 2008 have been linked to a range of oil and gas industry practices, including large-scale disposal of wastewater that can result in changes in subsurface stress and reactivation of preexisting faults (e.g., Ellsworth, 2013; Rubinstein & Mahani, 2015; Weingarten et al., 2015). In the state of Texas, earthquake rates at magnitude (M) 3 and above have risen from 2 earthquakes/yr (1975–2008) to 12 earthquakes/yr from 2008 through 2015 (Frohlich et al., 2016). There were nine M3+ earthquakes during 2016. The rate change in seismicity is largely associated with regions experiencing increased wastewater injection rates and volumes. Detailed studies related to post-2008 earthquakes in the Bend Arch-Fort Worth Basin (hereafter, FWB) (Frohlich, 2012; Frohlich et al., 2011, 2016; Hornbach et al., 2015, 2016; Justinic et al., 2013; Lund Snee & Zoback, 2016; Reiter et al., 2012) and East Texas Basin (Fan et al., 2016; Frohlich et al., 2014, 2016; Lund Snee & Zoback, 2016; Walter et al., 2016) suggest a link between earthquakes and saltwater disposal (SWD) operations at nearby injection wells. Extraction of unconventional shale gas and disposal of associated brines in the FWB dates to circa 1998 (Pollastro et al., 2007).

According to the Advanced National Seismic System Composite Earthquake Catalog (ANSS ComCat) (last accessed March 2017), earthquakes in the FWB began in October 2008 (Frohlich et al., 2016), and since that time, over 200 events have been reported over a 6,000 km^2 area that includes the Dallas-Fort Worth (DFW) metropolitan area of ~7 million people (Figure 1a). The first likely induced earthquake sequence occurred below the DFW International Airport and included an m_{bLg} 3.0 in 2008 and m_{bLg} 3.3 in 2009. A local seismic network deployed by Southern Methodist University (SMU) showed that earthquakes were spatially and temporally related to a nearby SWD well that began operations ~1.5 months prior to the first felt earthquake (Frohlich et al., 2011). While the physical mechanism linking the earthquakes to the SWD operations has been debated (Frohlich et al., 2011; Janská & Eisner, 2012; Reiter et al., 2012), the operator chose to voluntarily shut

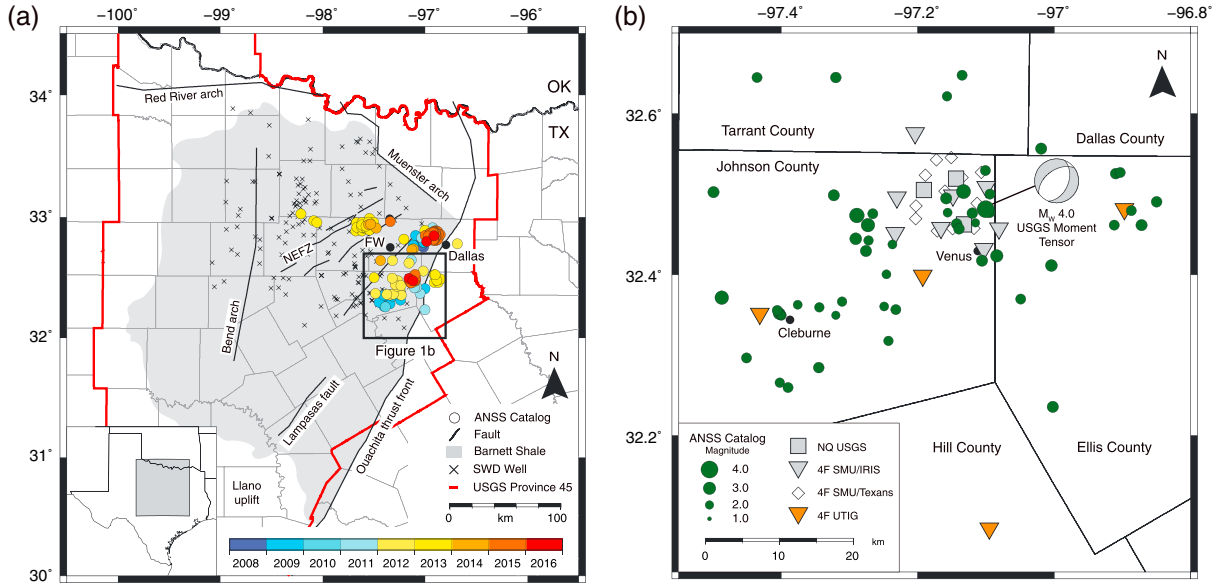

Figure 1. (a) Map of the Bend Arch-Fort Worth Basin, Texas (USGS Province 45), showing regional faults that have been inactive throughout the Quaternary (after Ewing et al., 1990), major structural features, and the extent of the Barnett Shale. ANSS ComCat earthquakes are colored by time (circles). SWD wells injecting brines into the Ordovician Ellenburger Limestone are shown (crosses). NEFZ: Newark east fault zone. FW: Fort Worth. The DFW metropolitan area includes the 12 counties that surround Dallas and Fort Worth. (b) Location map of the study area with the ANSS ComCat earthquakes (green circles) and the M_w 4.0 regional moment tensor. The temporary seismic network deployed in 2015 included rapid deployment of 14 Reftek125 "Texans" (diamonds) that were replaced by additional stations in late May 2015 (Data Set S1). Squares: USGS NetQuake accelerometers; triangles: SMU operated three-component short-period seismometers; orange triangles: UTIG operated broadband seismometers.

in the well in 2009. In June 2009, felt earthquakes occurred in Cleburne, a town located in central Johnson County, which had seen a rapid rise in SWD operations beginning in 2005 (Hornbach et al., 2016). Again, researchers concluded that nearby SWD operations plausibly triggered the Cleburne earthquakes (Justinic et al., 2013). Between 2009 and 2013, earthquakes continued in the FWB at variable rates, with magnitudes up to m_{bLg} 3.5. The passage of the Earthscope Transportable Array in late 2009 through early 2011 allowed lower magnitude seismicity to be documented in the basin (Frohlich, 2012).

Station density began increasing in the FWB in November 2013. At that time, a swarm of m_{bLg} 3.0+ earthquakes occurred over 2 months near Azle-Reno, northwest of the city of Fort Worth. SMU, in collaboration with the U.S. Geological Survey (USGS), deployed a new temporary seismic network and conducted subsurface pore fluid pressure modeling. Researchers concluded that a combination of SWD operations, potentially paired with water production at gas wells, most likely triggered seismicity on a preexisting fault (Hornbach et al., 2015). In 2015, additional seismic stations were put in the FWB to monitor a swarm of m_{bLg} 3.5+ events occurring on the border of the cities of Dallas and Irving and persistent seismic activity in Johnson County, resulting in continuous seismic network operations focused on ongoing earthquake sequences since late 2013 (DeShon & Magnani, 2016). The FWB is also routinely monitored by the TexNet Seismic Network [http://www.beg.utexas.edu/texnet] since late 2016.

Here we report on the 7 May 2015, M_w 4.0 Venus earthquake, so named due to the epicentral proximity to Venus, TX, in northeast Johnson County (Figure 1b). As of mid-2017, this event remains the largest earthquake recorded in the FWB. We present high-resolution earthquake locations and focal mechanisms derived using data from a local seismic network deployed in May 2015. Time-migrated, depth-converted seismic reflection data image the causative fault beyond the active seismic sequence and show fault offsets both in the basement and within the injection unit in the region. Template matching at permanent regional seismic stations indicates that earthquakes prior to the M_w 4.0, including some events reported by Frohlich (2012), likely occurred on the same fault. We show that the fault hosting the M_w 4.0 Venus earthquake has been active since 2008 and is characterized by increasing maximum magnitude events with time, similar to seismicity trends noted at other injection-induced areas such as Paradox Valley (e.g., Yeck et al., 2015). The 2008 onset of seismicity is slightly delayed relative to the onset of SWD operations in northeast

Johnson County in 2006. This activity consists of five SWD wells operating within 100 km^2 of the sequence, with different start times and histories. Analysis of aggregated data from these wells indicates that significant overpressure exists in the injection unit as of 2015. The combined analyses of seismic and injection data support the hypothesis that SWD increased subsurface fluid pressure for nearly a decade, promoting failure on the fault associated with the Venus earthquake.

2. Geologic and Seismic History

The FWB is a shallow northeast-southwest elongated foreland basin that contains the Mississippian Barnett Shale, the source unit for the unconventional shale oil and gas play (Pollastro et al., 2007). The basin is associated with the rising of the Ouachita orogenic belt during the Late Paleozoic phases of the diachronous assembly of the supercontinent Pangaea (Thomas, 2006). It is a synclinal structure that deepens to the northeast and parallels the Ouachita thrust front, which bounds it to the east. To the north, the basement-controlled Muenster arch structurally limits the basin, while to the west and south, the basin shallows toward the Bend arch and Llano uplift, respectively (Figure 1a).

East of the Bend arch, in the deepest part of the basin, the thick clastic sequences of the Pennsylvanian Bend and Strawn Group rest upon the stratigraphically thin Mississippian shales and carbonates, and on the Ordovician carbonates, which dip eastward toward the Ouachita thrust front (Kier, 1988). Seismic reflection data across the Ouachita thrust front region show a system of high-angle normal faults displacing the Ordovician platform and shale strata toward the east, under the Ouachita orogen, where the signal of the deeper units is lost (Thomas et al., 1989).

Beneath northeast Johnson County near Venus, wells encounter the top of the Precambrian, granitic basement at ~3.9 km depth (e.g., Pollastro et al., 2007). The dolomite of the Ellenburger Limestone—an Ordovician carbonate platform deposit used as a wastewater disposal unit throughout the FWB since 2005—rests unconformably over the basement. The top of the Ellenburger Limestone is approximately 2.5 km deep, and the unit is ~1.4 km thick in the Venus area, dipping gently to the east. The Ordovician Chappel Limestone, Viola Limestone, and Simpson Group lie between the Ellenburger Group and the Mississippian gas-producing Barnett Shale. These Ordovician stratigraphic elements are a critical boundary in the Barnett Shale gas play, as they are not ubiquitous in the FWB, and where they are not present the unconventional production unit of the Barnett Shale rests directly over the water-saturated, high-permeability carbonates of the Ellenburger. The Viola-Simpson Group has been identified in the subsurface along the eastern part of the FWB, and in boreholes in eastern Johnson County near Venus (Pollastro et al., 2007). In this area, the unit is relatively thin (~50 m) and thins westward, beneath the ~100 m thick Barnett Shale. The top of the Barnett Shale is detected in 3 well logs in the study area at about 2.45 km depth.

The Texas Railroad Commission (TRC), the oil and gas regulatory agency in Texas, reports over 15,000 production wells associated with the Barnett Shale in the FWB. The Barnett Shale hydraulic fracturing process typically involves 11,000–19,000 m^3 (69,000–119,000 barrels) of water for each well (Nicot et al., 2014), and fluids produced with gas are a mix of flowback of fracture (frac) fluids and natural brine associated with the formation (see Hornbach et al., 2016, for discussion). This wastewater is disposed of via injection at Class II UIC SWD wells into deep, saltwater bearing permeable units. The FWB has more than five SWD wells every 5 km^2, making it one of the densest regions of active SWD wells in the United States (Weingarten et al., 2015). Since 2005, over 305×10^6 m^3 (1.9 billion barrels) of wastewater have been injected into the Ellenburger, which serves as one of the primary injection targets in the basin. Peak injection volumes in the FWB occurred in 2014 (208 million barrels), with the total volume reported for 2016 (107.5 million barrels) approaching the total volume reported circa 2007 (109.2 million barrels) (TRC Website, last accessed April 2017).

Based on the ANSS ComCat, Johnson County has exhibited prolonged seismic activity spanning 2009–2016, and the earthquakes can be grouped into four spatial clusters (Figure 1b): (1) south-central Johnson County near the town of Cleburne, TX; (2) central Johnson County; (3) northeast Johnson County, north of the town of Venus, TX; and (4) east Johnson County/northwest Ellis County. Central Johnson County activity began in 2012, while the region near the eastern border of Johnson County and northwest Ellis County was active in 2011. Unfortunately, the lack of local seismic stations limits our ability to characterize these sequences. In northeast Johnson County, the first ANSS ComCat earthquake was reported in 2013. Using data from

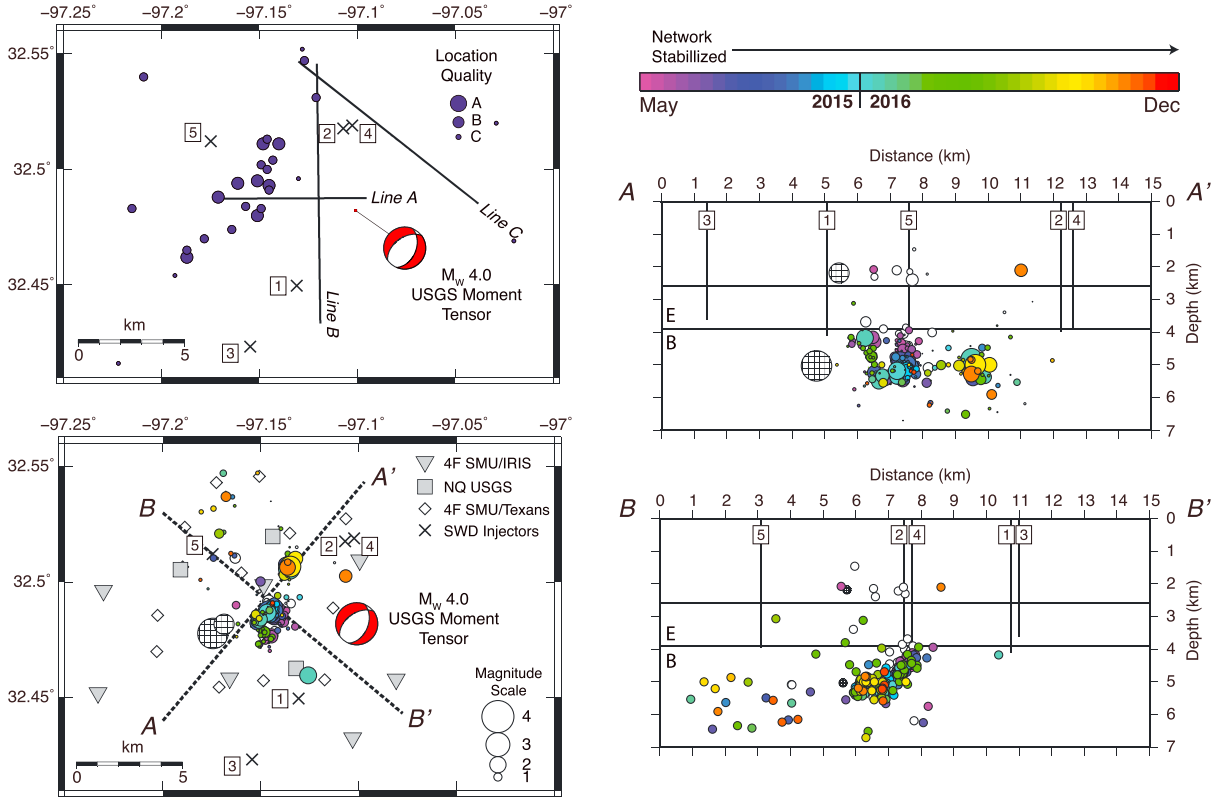

Figure 2. (top left) Location map of seismic reflection profiles (Lines A, B, and C) near Venus, TX. The five nearest SWD wells (numbered squares) are labeled 1 (earliest) to 5 (latest) according to onset of injection activity. Circles are the Frohlich (2012) earthquake catalog scaled by reported quality. NEIC moment tensor points to the ANSS ComCat location of the M_w 4.0 earthquake. (bottom left) Enlarged view of northeast Johnson County showing locations of earthquakes in the local catalogs, temporary seismic stations, and locations of the SWD wells. Earthquakes in the SMU catalog (white and colored circles) are scaled by magnitude. For the SMU catalog: the M_w 4.0 and m_{bLg} 2.4 aftershock were recorded on SMU-operated stations within the FWB but at regional distances (checkered circles); 26 earthquakes were recorded by the "Texans" (white circles); and the remaining 279 earthquakes (colored by time) were recorded after network geometry stabilized in late May 2015. NEIC moment tensor is placed at the ANSS ComCat solution for the M_w 4.0 Venus earthquake. (right) Cross sections along A-A′ and B-B′ with symbols as described previously. Earthquakes and SWD wells are projected onto A-A′, with earthquakes scaled by magnitude; earthquakes projected onto B-B′ are not scaled by magnitude for better fault interpretation. Geologic units discussed in the text are labeled.

the EarthScope Transportable Array, Frohlich (2012) located 32 events in this area during the time period 2009–2011.

The M_w 4.0 Venus earthquake occurred on 7 May 2015, at 22:58:05.200 UTC (16:58:05.200 CST) at a reported depth of 2.5 km (Figure 1b). Over 600 felt reports ranging from 5 km to as far as 200 km away were associated with the event (USGS "Did You Feel It?," last accessed March 2017). The strongest shaking—a Modified Mercalli Intensity (MMI) IV (light shaking)—was felt in an area of low population density, with ~64,000 people within a radius of 17 km of the reported epicenter. An estimated 7.6 million people were exposed to weak shaking (MMI: II-III) (USGS ShakeMap, last accessed March 2017). There were no fatalities and no reports of economic loss from the earthquake. Analysis of the SMU seismic network, then centered around Azle-Reno and Irving/Dallas northwest and north of Venus, yielded near colocation of the M_w 4.0 and the first m_{bLg} 2.4 aftershock. The SMU locations were ~7 km west of the USGS location for the M_w 4.0 (Figure 2).

3. Data Sets

3.1. Earthquake Data

3.1.1. Network Operations and Local Earthquake Catalog

A temporary seismic network was deployed in two stages beginning 3 days following the M_w 4.0 Venus earthquake (Figure 1b). Initial deployment consisted of 14 vertical-component RefTek 125 seismometers "Texans" (Data Set S1 in the supporting information) that remained in place through 17 May 2015. SMU then deployed

three USGS NetQuakes accelerometers and seven, 3-component short-period stations provided by the Incorporated Research Institutes for Seismology (IRIS) (Data Set S1). Station configuration was designed to optimize earthquake location and focal mechanism resolution for small magnitude (<2.0) events. Concurrently, the University of Texas Institute for Geophysics (UTIG) deployed four broadband stations (Data Set S1) sited at greater distances throughout Johnson and Ellis Counties, in part to provide better monitoring capabilities across the southern FWB. Stations are sampled at either 100 or 200 samples per second (Data Set S1). The SMU/UTIG network geometry was static over the time period of this study (May 2015–December 2016), though station uptimes varied. Data from the SMU-operated stations were, and continue to be, telemetered for daily analysis and archived directly to the IRIS Data Management Center. Data from UTIG stations were not telemetered until 2017. All continuous waveform data are archived under Federated Digital Seismic Network (FDSN) codes 4F (SMU/UTIG) and NQ (USGS NetQuakes). Network geometry was significantly modified in January 2017 with the incorporation of the TexNet Seismic Network stations (FDSN: TX), merging of UTIG stations into TexNet, and demobilization of USGS NetQuakes instruments.

The SMU earthquake catalog based on local distance data is built within the Antelope processing package (Boulder Real Time Technologies, Kinemetrics) using GENLOC location algorithms (Pavlis et al., 2004). All events are located using 1-D velocity models developed for the FWB (Text S1 and Figures S1–S3), and we use a local magnitude calculator calibrated to the ANSS ComCat m_{bLg} following the method of Walter et al. (2016) (Figure S4). Additional details regarding the SMU catalog and associated uncertainties are presented in the supporting information (see Text S1).

As of December 2016, 301 earthquakes have been detected and located using the local seismic network (Figure 2 and Data Set S2). Uncertainty ellipses estimated at the 68% confidence level have a median major (minor) length of 0.17 (0.10) km. Median uncertainties in origin time and depth are 0.02 s and 0.14 km, respectively. The median root mean square (RMS) time is 0.05 s. Most earthquake uncertainty ellipses exhibit a strike between 5°N and 40°N. While these formal uncertainties are likely underestimated because of unmapped error associated with the 1-D velocity model, the small values reflect the high-quality data set and associated locations. Event magnitudes range from −0.5 to 4.0 M_L and have an average of 7 *P* and 7 *S* wave onsets. The May 2015 M_w 4.0 and m_{bLg} 2.4 aftershock have higher location uncertainties because they were located using the stations 40–60 km to the north and northwest. The 26 small earthquakes recorded by the one-component stations also have larger hypocentral uncertainties, especially in depth due to lack of quality onset times for *S* waves (see Figure S5 for catalog locations with uncertainty bars and Data Set S2).

Only seven earthquakes in the SMU catalog for northeast Johnson County are found in the ANSS ComCat. The ANSS ComCat appears complete to m_{bLg} 2.8 in northeast Johnson County, whereas the local earthquake catalog is complete to M_L 0.5 based on frequency-magnitude relationships (Scales, 2017). The USGS National Earthquake Information Center (NEIC) calculated a moment tensor solution for the M_w 4.0 earthquake, presented in Figure 2. The strike, dip, and rake of the nodal planes are 22°, 45°, −114° and 234°, 50°, −68° dipping to the southeast and northwest, respectively. A solution was also estimated at Saint Louis University (SLU) (Herrmann, 2013); the strike, dip, and rake of the nodal planes were 19°, 46°, −117° and 235°, 50°, −65°, which are consistent with the moment tensor provided by the NEIC.

In the SMU catalog, earthquakes appear associated with a single linear structure that extends ~5 km in length and exhibits a strike NE-SW with a NW dip. This planar feature is consistent with the 234–235° striking nodal plane reported in the moment tensors and is interpreted as the causative fault. SLU also identified this plane as the preferred fault plane based on a combination of spectral and waveform data. Most earthquakes locate between 4 and 6 km depth and are consistent in depth with faulting in the Precambrian basement (Figure 2). The SMU catalog locations are also spatially coincident with earthquakes identified in northeast Johnson County by Frohlich (2012) (Figure 2). Earthquakes are not limited to a single structure; however, with the addition of stations in the area, we document earthquakes to the NW and one event to the SE (Figure 2). Earthquakes that appear within the Ellenburger are associated with higher uncertainty in location than earthquakes within the basement.

3.1.2. Matched Filter Technique

Prior to the M_w 4.0 earthquake, there were no seismic stations located close enough to detect precursory seismicity below ~*M*2.4. To document any initial seismicity in the region, we utilized a matched filter technique on regional seismograms. This method assumes earthquakes that generate similar waveforms have similar

source parameters, including spatial proximity. Matched filter techniques have been widely implemented to detect repeating seismic events, including triggered earthquakes (Meng et al., 2013), induced seismicity (Skoumal et al., 2014; Walter et al., 2016), foreshocks prior to large megathrust earthquakes (Kato et al., 2012; Walter et al., 2015), and aftershocks (Meng et al., 2013). We followed the matched filtering process designed to study the 2014 Timpson, TX, earthquake sequence in east Texas (Walter et al., 2016). Templates were compared to continuous waveforms recorded at all regional stations from January 2002 to December 2015. Template earthquakes were limited to all ANSS ComCat (including the M_w 4.0) and Frohlich (2012) epicenters near Venus (32.45–32.54°N and 97.2–97.08°W). Further processing details are included in the supporting information (Text S2). The resulting matched filter catalog provides information on earthquake time history but does not provide reliable hypocenter locations.

3.1.3. Double-Difference Relocation

We computed high-resolution double-difference (DD) earthquake locations to gain a better understanding of the seismogenic behavior of the causative fault. The DD location method uses differences in travel times (differential times) to solve for relative earthquake locations under the assumption that seismic waves from earthquakes in close spatial proximity travel along similar ray paths and hence the relative arrival times map directly to spatial separation (Waldhauser & Ellsworth, 2000). We used the *tomoDD* application of the DD approach (Zhang & Thurber, 2003) and use the University of Alaska Geophysical Institute's Seismology Matlab Objects Suite for MATLAB (Reyes & West, 2011) to perform the cross correlation to yield more accurate differential times for similar waveform pairs. The DD relocation approach, with event waveform correlation, was applied to the SMU catalog for northeast Johnson County. We used a gradient version of the 1-D model (Figure S1) used within Antelope and only incorporate phase data recorded at local distances. This limits analysis to the ~300 small magnitude earthquakes. Details on the parameterization choices within each software package are provided in the supporting information (Text S3). Additionally, description of the wide range of tests to assess relative and absolute location accuracy is detailed in the supporting information (Text S3) and in Scales (2017).

3.1.4. Focal Mechanism Technique

Focal mechanisms were constrained by *P* wave first-motion polarity and *S* to *P* amplitude ratios (*S*/*P*). We used a program developed by Hardebeck and Shearer (HASH), which generates focal mechanisms while accounting for uncertainties in the velocity model, earthquake locations, and *P* wave polarities (Hardebeck & Shearer, 2002, 2003). In northeast Johnson County, individual *P* wave first-motion solutions could not be generated for many earthquakes because they lacked station coverage, had low signal-to-noise ratios, and/or had emergent phases. Inclusion of *S*/*P* data helped improve quality of the focal mechanism data set (i.e., Shen et al., 1997). Amplitude measurements were limited to earthquakes that were located using a minimum of six, 3-component seismic stations with a signal-to-noise ratio greater than 3 (Hardebeck & Shearer, 2003) and calculation of *S*/*P* amplitude followed standardized procedures outlined in Hardebeck and Shearer (2003) (see Text S4 for further detail). Mechanism quality was rated according to RMS fault plane uncertainty: A (RMS uncertainty $\leq$25°), B (RMS uncertainty $\leq$35°), and C (RMS uncertainty $\leq$45°).

3.2. Seismic Reflection Data

A total of 32 km of 2-D seismic reflection data were analyzed and interpreted (Figure 2) in order to provide a tectonic and structural context of the study area, to identify and constrain the fault geometry (e.g., length, dip, and strike), and to constrain the history of deformation on faults in northeast Johnson County. These data were acquired in 1964 (Line C) and 1974 (Lines A and B) using dynamite sources and recorded to a maximum length of 7 s travel time. The data were originally processed to time stack sections and later reprocessed to improve the stack and apply time migration (Line C in 2010 and Line B in 2015). All data were purchased as poststack; prestack analysis could not be performed. Frequency content analysis indicates that the resolution of the data is ~10 m at 0–2 km depth and ~15 m from 2 to 4 km depth. Lines A and B were time-migrated, and all profiles were depth converted in order to compare earthquake hypocenter locations and imaged features. For consistency with earthquake locations, the 1-D velocity function used for time-to-depth conversion was derived from the gradient velocity model used for seismicity relocation (Figure S1), and depths were calibrated on well log depths of the regional stratigraphic boundaries in the area. The tops of the main stratigraphic units were identified on well logs using gamma ray and resistivity information, when available. The well log picks were then projected onto the nearest seismic profile and correlated with reflectors, and the

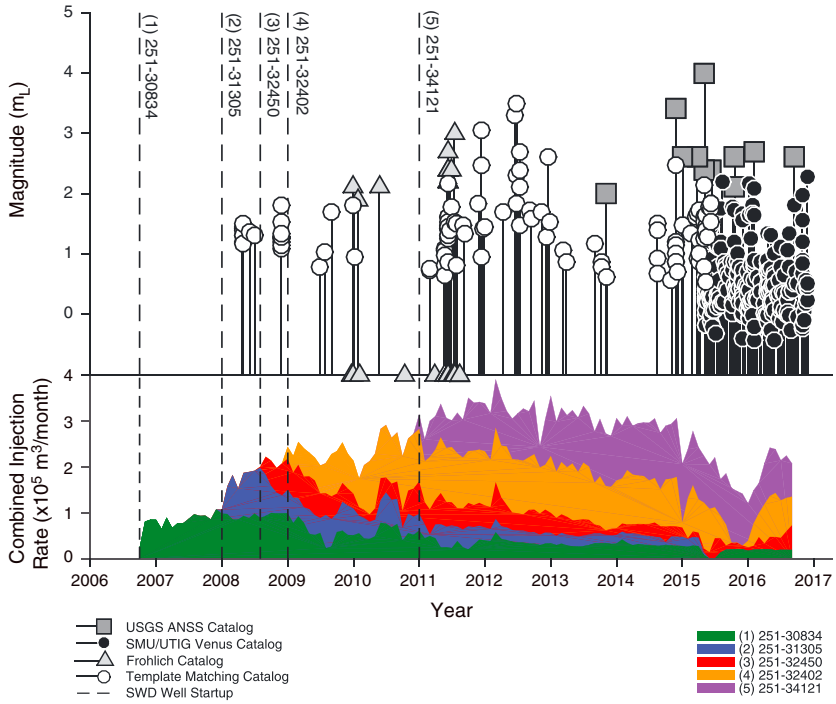

Figure 3. (top) Earthquake magnitudes from 2008 through the end of 2016. The matched filter detections (white circles), Frohlich (2012) catalog (gray triangles), ANSS ComCat (gray squares), and SMU catalog (black circles) show increasing maximum magnitude with time. Note that some Frohlich (2012) catalog earthquakes do not have reported magnitudes. ANSS ComCat solutions within 5 km of the SMU solution for the M_w 4.0 are included. The 5 SWD wells (shown in Figure 2) began operations starting in late 2006 (dotted lines) and are labeled numerically by start date order and by API number. (bottom) Monthly injection volumes of the five nearest SWD wells over time. Colors show the contribution of an individual injection well volume to the total volume of all five wells.

interpretation propagated to the intersecting seismic profiles at crossing points to provide an internally consistent interpretation.

3.3. Injection Well Information

The TRC requires monthly injection volumes for each well to be reported annually in October. As of 2016, these data indicate 27 disposal wells (of 39 with active permits) in Johnson County. From 2005 to 2016, these wells injected a combined total of over 1.25×10^8 m^3 (790 million barrels) into the Ellenburger, making Johnson County the highest injection volume per unit area in the FWB (e.g., Hornbach et al., 2016). The five injectors located within 6 km of the M_w 4.0 Venus earthquake account for 2.8×10^7 m^3 (175 million barrels) through September 2016. The five wells were shut down following the Venus earthquake to conduct falloff testing to determine background pressure levels (i.e., the state of pressure within the injection unit without active injection occurring), with data made publically available (Text S5–TRC Website 1). Injection resumed at all wells after testing was completed in May 2015. This study analyzes the five nearest wells to the sequence because of proximity and falloff data availability. It is important to note that pressure observations of the injection unit are likely influenced by most, if not all, wells near northeast Johnson County and far-field effects from more distant wells cannot be ruled out.

4. Results

4.1. Earthquake Data

4.1.1. Matched Filter Catalog

Using the matched filter technique, we identify earthquakes at the *M*1.0 level and above beginning in 2008 and occurring fairly regularly, up to and including the M_w 4.0 sequence in 2015 (Data Set S3). Only two brief periods of quiescence in late 2010 and early 2014 are identified. The matched filter results suggest at least two foreshocks within 24 h of the Venus earthquake: a M_L 1.3 earthquake ~12 h prior and a M_L 2.2

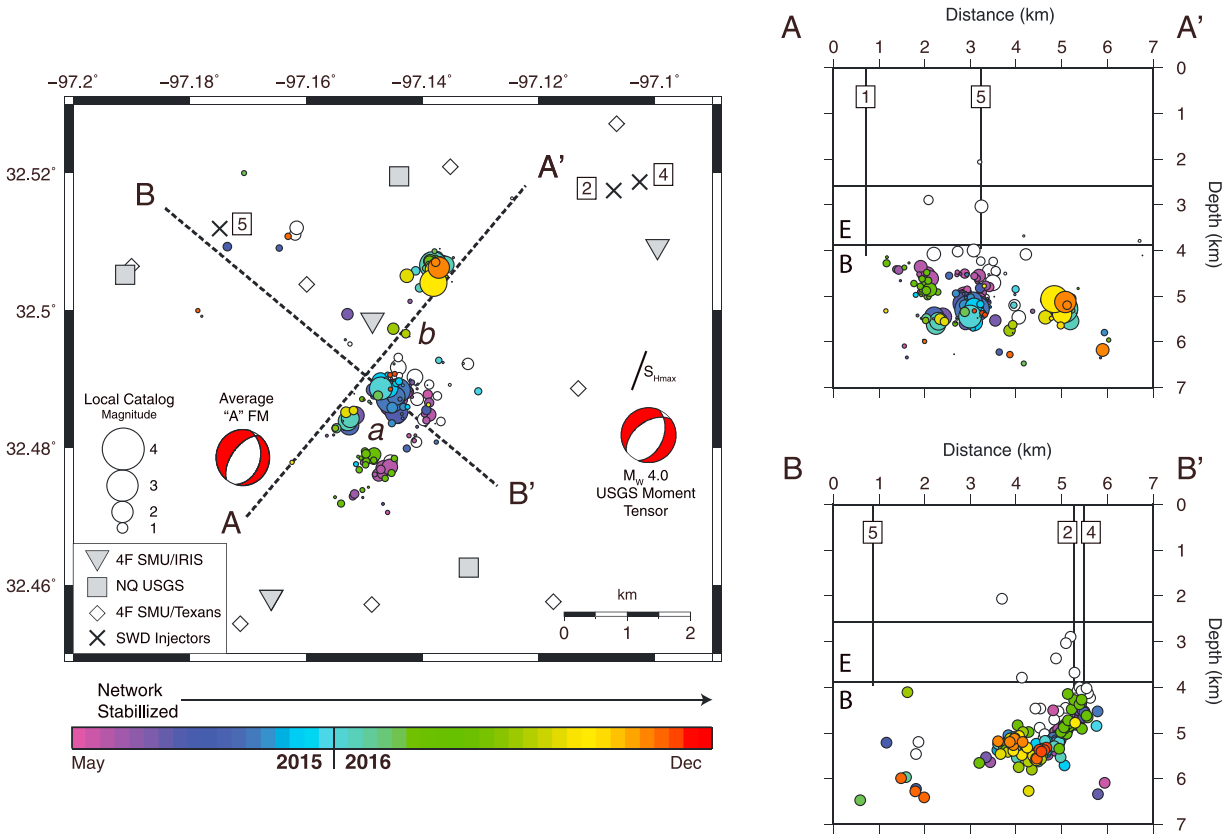

Figure 4. *Map view*: Earthquake locations in the high-resolution DD catalog. Labeling follows Figure 2. The NEIC moment tensor is placed at the ANSS ComCat location for the M_w 4.0 earthquake. The average "A" quality focal mechanism is placed at the SMU catalog location for the M_w 4.0 earthquake. Seismic gaps discussed in the text are labeled *a* and b. *Cross section*: Cross sections along A-A′ and B-B′ with labeling also following Figure 2. E: Ellenburger; B: Basement.

earthquake ~2.5 h prior that were not detected by the SMU network operating in Azle and Irving. The onset of earthquake activity in 2008 is consistent with the beginning of operations at two of the nearby SWD wells (Figure 3). The M_w 4.0 occurred ~7 years after injection operations began and ~1.5 years after peak injection volumes (as of 2016) were reached.

4.1.2. DD Catalog

Of the 301 earthquakes, 286 were relocated using *tomoDD* (Figure 4 and Data Set S4). The DD catalog absolute uncertainty estimate is 0.32 km in epicenter, 0.35 km in depth, 0.30 s in origin time, and 0.03 s in RMS (see Text S3 for uncertainty determination). The DD catalog reveals a basement fault that is 5 km long, extending 4–6 km in depth, with a NE-SW strike and NW dip (Figure 4). Initial small magnitude aftershocks (purple and blue circles in Figure 4) occur at the updip edge of the fault and wrap around an apparent seismic gap (labeled *a* in Figure 4) to fill in the downdip edge of the rupture plane. Over time earthquakes propagate further to the northwest but rarely if ever (given location uncertainty) occur into the area labeled *b* in Figure 4. Based on the location of the initial aftershocks, and the observation that initial aftershocks frequently focus on the edges of highest slip (Beroza & Zoback, 1993), we suggest that slip in the M_w 4.0 earthquake likely occurred in the southwest seismic gap. However, we cannot rule out that slip during the M_w 4.0 occurred in the northeast gap nor speak to the fine details of slip distribution from 2008 to May 2015. The DD catalog confirms that slip after May 2015 is confined to the basement rocks and extends to within 1 km of the deepest injection intervals (Figure 4).

One significant aspect of the seismicity is that when viewed in a strike-perpendicular cross section (Figure 4, B-B′), the earthquakes do not collapse onto a linear dipping feature. A perfect linear planar fault should appear as a line when viewed in strike-perpendicular cross section, and instead, the apparent double dipping feature indicates geometric complexity or multiple faults. Fault geometry is explored further using analysis of seismic reflection data below.

4.1.3. Focal Mechanism Solutions

Using *P* wave first motions and *S*/*P* data, we generated a total of 49 focal mechanisms for northeast Johnson County (Figure S6 and Data Set S5) with most indicating primarily normal faulting on NE-SW striking faults. Individual mechanism quality is variable with 9 ranked as A, 31 as B, 7 as C, and 2 as D. The median strikes of both nodal planes of all solutions are 220°N ± 20° and 335°N ± 24° with the median dips of nodal planes being 57°NW ± 7° and 42°NW ± 5°, respectively. These values are consistent with the NEIC moment tensor solution, SLU moment tensor solution, and catalog locations, as well as previous studies conducted in the FWB (Hornbach et al., 2015; Justinic et al., 2013). A recently published stress map of Texas documents maximum horizontal compressive stress ($S_{H\max}$) in the FWB at ~20°N (Lund Snee & Zoback, 2016). This orientation lies within the median absolute deviation of the median strike of the calculated nodal planes within the Venus area. Based on DD locations, we interpret the causative fault of the M_w 4.0 earthquake to be the nodal plane with a strike of 220°N and dip 57°NW.

4.2. Seismic Interpretation

The seismic reflection profiles image the stratigraphy of the FWB from the Pennsylvanian-Cretaceous unconformity, traceable at a depth of ~500 m, to the high-amplitude discontinuous reflector marking the top of the Precambrian crystalline basement at a depth of ~4 km. The Mississippian and Pennsylvanian shales and limestones (Chappel, Barnett, and Marble Fall Formations) are clearly imaged between ~2.25 and 2.75 km as a sequence of bright and continuous reflectors, above the transparent, 1.5 km-thick Ordovician carbonates. The granodioritic Precambrian basement rocks appear featureless and transparent on Lines B and C. East dipping basement reflectors are visible on the west end of Line A, at a depth of ~6.5 km, suggesting that the lack of reflectivity, within basement rocks, is likely due to tight folds and pervasive deformation rather than a lack of energy penetration. The basement and overlying Ordovician-Mississippian sequences dip gently to the east, toward the Ouachita thrust, showing the generalized flexure of the basin under the orogenic belt (Pollastro et al., 2007; Thomas, 2011; Thomas et al., 1989). The transition from the Lower Pennsylvanian limestones (Marble Falls Formation) to the clastic rocks of the foredeep basin (the Atokan portion of the Bend Group) is marked by an angular unconformity that is clearly visible on Line B and Line C. The Middle Pennsylvanian basin fill (Bend and Strawn Group) exhibits a northward dip, possibly indicating a northward prograding environment with sources from the Ouachita fold and thrust belt uplift to the southeast. At the tops of the profiles, the southeastward thickening Mesozoic Gulf Coastal Plain sediments rest unconformably on the Pennsylvanian foredeep facies.

The Paleozoic rocks of the FWB appear to be mildly deformed in this area, and the seismic data image two previously unpublished main faults, named herein the Western Venus fault (WVF) and Eastern Venus fault (EVF) (Figure 5). The faults offset the crystalline basement, the Ordovician carbonates, the Mississippian limestones and shales, and penetrate the Marble Falls Formation. The faults appear to terminate below or in the Middle Pennsylvanian units, within which the seismic data resolve no apparent offset of strata.

The EVF can be interpreted on Lines A and C as steeply east dipping, striking approximately 25°N with an antithetic west dipping splay. The faults are traceable from the top of the basement into the Ellenburger Limestone, through the Mississippian shales to the top of the Marble Falls Formation. Strata appear to be downdropped between the two fault splays, suggesting they deformed during extension or form a small graben within a strike-slip system. The interpretation of the EVF along Line B is more problematic. The top of basement, top of Ordovician carbonates, and top of Pennsylvanian limestones appear to be folded along the southwest projection of the EVF onto Line B, but no offset is evident. We therefore interpret the fault to extend to Line B with a decreased displacement and suggest that deformation might eventually fade to the southwest or/and be transferred to another adjoining structure. The EVF, as interpreted on the seismic profiles, is at least a 7.5 km-long structure.

The expression of the WVF is subtler than the EVF. Reflector offsets are limited to few tens of meters at the Mississippian shale reflector, and the position of the fault is derived from concurrent evidence of hanging wall deformation, offset/reflector truncation, and diffracted energy at the top of the crystalline basement (Figure 5). The WVF so interpreted is at least a 6.5 km-long or longer, west dipping fault with a down-to-the-west sense of motion. The fault cuts the basement and Paleozoic rocks from the Ordovician limestones to the Mississippian shales but shows no evidence of displacement at the top of the Pennsylvanian Marble

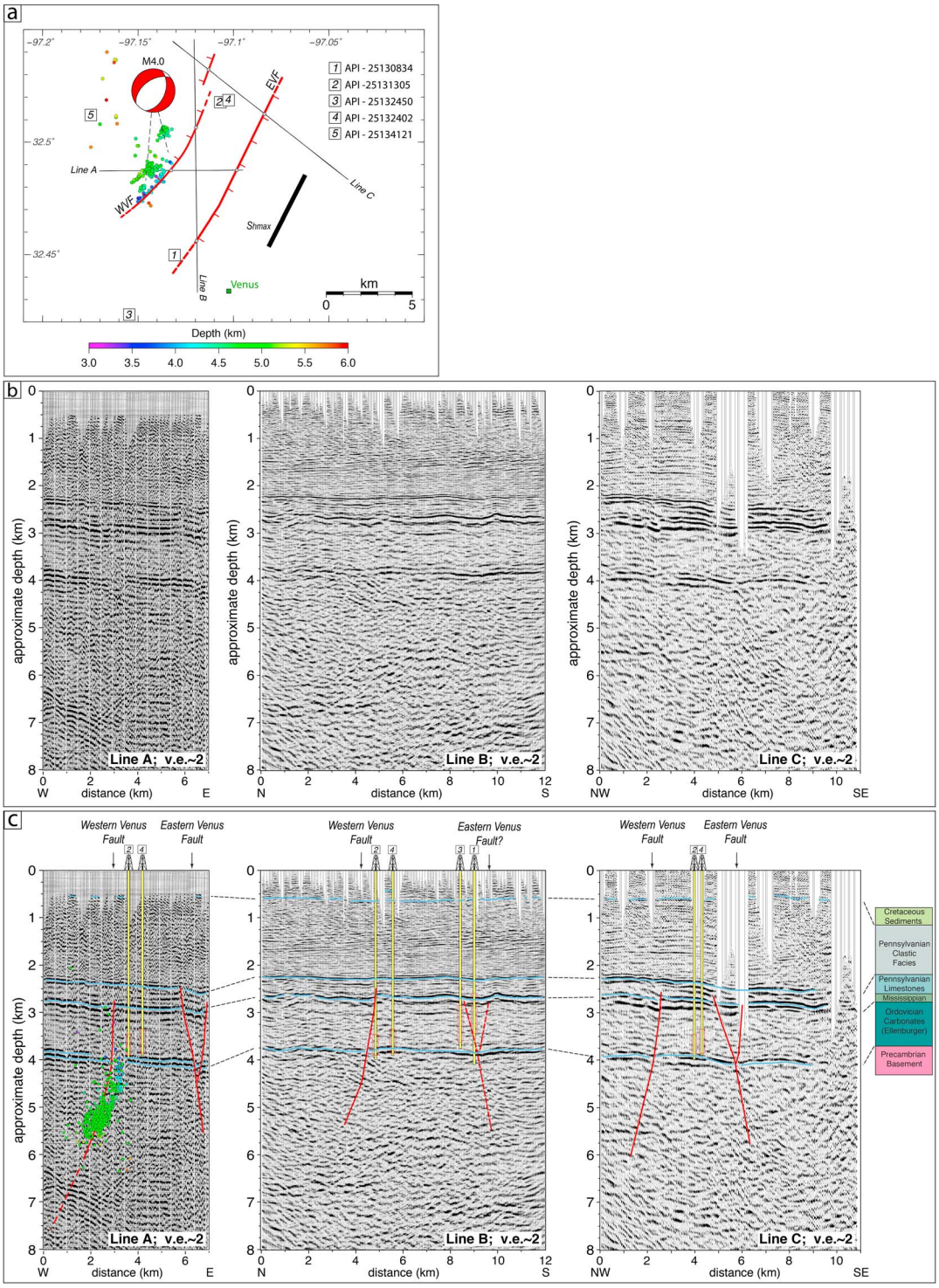

Figure 5. (a) Location map of seismic reflection profiles (Lines A, B, and C) near Venus, TX. Faults interpreted on the reflection data are shown at the top of the basement (EVF: Eastern Venus fault; WVF: Western Venus fault). The WVF has been reactivated during the 2008–2017 seismic sequence in northeast Johnson County. Squares represent the five SWD wells discussed in the text; circles are the DD catalog color coded by depth; regional stress orientation of $S_{H\max}$ ~ 20°N (black line) (Lund Snee & Zoback, 2016); NEIC moment tensor for the M_w 4.0 points to seismic gabs *a* and *b* discussed in the text. (b) Time-migrated, depth-converted seismic reflection profiles without interpretation. (c) Time-migrated, depth-converted seismic reflection profiles with interpretation overlay, projected well locations (projected along regional structural trend), injection intervals (red rectangles on wells), and hypocentral locations (green circles). The seismic reflection data imaged the faults cutting the crystalline basement and the Ordovician and Mississippian units but do not show offset above the Pennsylvanian limestones (Marble Falls Formation). See text for detailed description of stratigraphy and structural interpretation. After Magnani et al. (2015). All sections shown at approximately 2:1 vertical exaggeration. Seismic data owned or controlled by Seismic Exchange, Inc.; interpretation is that of U.S. Geological Survey and SMU.

Table 1
Information for the Five SWD Wells Discussed in the Text

	Ferguson[a] (1)	Kimbrough[a,b] (2)	Highway 67[c] (3)	Metro (4)	Sophia[d] (5)
API well number	25130834	25131305	25132450	25132402	25134121
Drill depth (m)	4114.80	3989.83	3749.04	3908.45	3962.40
Top injection depth[e] (m)	2607.56	3462.53	2847.14	3369.87	2743.20
Bottom injection depth[e] (m)	3461.31	3875.84	3619.80	3870.10	3962.40
Estimated bottom hole pressure[f] (MPa)	1.7	0.9	1.52	4.84	2.34
Absolute bottom hole pressure (MPa)	N/A	N/A	37.45	N/A	N/A
Absolute bottom hydrostatic pressure[g] (MPa)	34.36	38.48	35.94	38.42	39.34

[a]Falloff data needed to be digitized. There is a larger uncertainty associated with these values. [b]Falloff data never reach a steady state condition. Bottom-hole pressure is extrapolated via a linear least squares fit to the log-log data. [c]Absolute bottom hydrostatic pressure is used for correction to relative pressure seen in Figure 6. [d]Well documentation not publicly available. Drill depth selected based on TRC e-mail (Text S5—TRC Website 2 (4)). Injection interval is the permitted injection interval as no information for perforation zone is reported. The data from the TRC already report altered injection intervals for this well (Text S5—TRC Website 2 (5)). [e]Top and bottom of injection interval are chosen as the minimum and maximum depth of the reported perforation zone, respectively. Well 1 is the only well reporting multiple perforation zones (Text S5—TRC Website 2). [f]Estimated bottom hole pressure values are calculated using falloff tests. Values are taken from the steady state portion (the pressure at which the change in pressure with time goes to 0) of the falloff test. [g]Hydrostatic pressure calculated using $P = \rho gh$ at depth of interest.

Falls Formation; however, the reflector that marks the top of the formation appears to be gently folded over the fault in Line C, suggesting mild tectonic activity at this time. The Bend Group sedimentary rocks above the Lower Pennsylvanian sequences appear undeformed wherever they are well imaged. Based on the constraints from the seismic reflection data, the WVF strikes ~210°N between Lines A and B and either rotates to ~192°N between Line B and Line C, indicating a curved fault geometry, or ends east of Line B. The strike of 210°N between Lines A and B is consistent with focal mechanisms and moment tensor solutions (220°N to 235°N).

4.3. Injection Analysis

A summary of the injection well parameters and falloff test interpretation is provided in Table 1. Well 3 reported background pressures of ~37 MPa (~5,432 pounds per square inch, PSI), while the other four wells reported pressures of 1.4–4.0 MPa (200–600 PSI). Because Well 3 is significantly closer to hydrostatic pressure (37 MPa) than the other four wells, we assume the four wells reported pressure relative to hydrostatic and corrected well 3 to yield the same measurement (Figure 6 and Table 1). The falloff tests that occurred at the five disposal wells immediately following the M_w 4.0 event indicate overpressures within the injection interval of each well ranging from 0.9 to 4.8 MPa (Figure 6) above hydrostatic.

The excess pressures observed in the Venus falloff tests are far greater than the 0.01–0.2 MPa (above hydrostatic) pressure values modeled for Azle, TX (Hornbach et al., 2015) or basin wide estimates of pressure increase within the Ellenburger (~0.09 MPa) due to a decade of wastewater injection (Hornbach et al., 2016). However, the observed Ellenburger pressures around Johnson County from falloff tests are comparable to what we would predict if all fluids injected into the Ellenburger from wells located within the county were confined only to the county (Figures 6 and S7). Additional modeling work for Johnson County, presented in Gono et al. (2015), also predicts pressure increases similar to results from the falloff tests (Figure 6). Johnson County has served as a focus of significant injection activity across the FWB during the shale gas revolution (e.g., Frohlich, 2012; Hornbach et al., 2016).

We see no definitive spatial or temporal correlation between individual well injection start times, rates, or volumes, and the earthquake space and time history. Efforts to document earthquake location diffusion away from wells using the Frohlich (2012) and SMU catalog yielded inconclusive results. We observe a general temporal and spatial relationship between seismicity and the combined pressure change within the injection unit over the last decade (Figure S7). We also observe that increasing maximum magnitude with time is linearly correlated with logarithm of the cumulative injected volume (Figure S8), similar to the relationship noted for induced earthquakes in Paradox Valley (Yeck et al., 2015). The Ellenburger Limestone is a heterogeneous karsted dolomite/limestone (Sullivan et al., 2006), and based on current data, we suggest that earthquakes are likely induced by the cumulative injection activity in this area, rather than individual wells or subsets of the nearest wells.

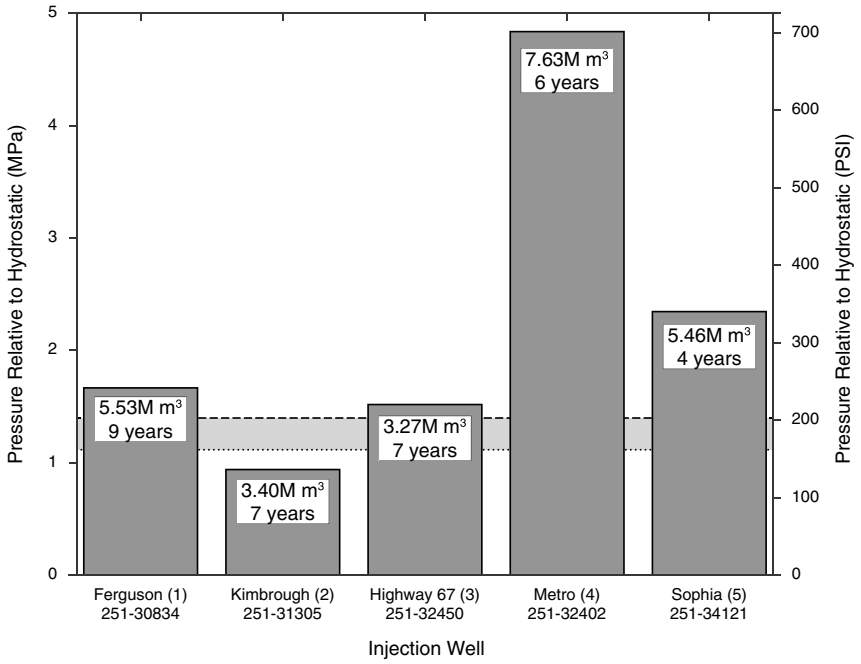

Figure 6. Data from the falloff tests for five SWD wells showing measured, sustained pressures, total volume injected and duration of injection prior to May 2015. Falloff tests were performed after the M_W 4.0 May 2015 earthquake. Numbering (1–5) for this study corresponds to onset time. Gray shaded area shows range of modeled pressure increase above hydrostatic caused by injection of these five wells (dashed line, Gono et al., 2015) and calculated (dotted line, Figure S7) for Johnson County. Additional information on each well is documented in the supporting information.

5. Discussion

Northeast Johnson County earthquakes document nearly a decade-long seismogenic evolution of a reactivated intraplate fault. The northeast Johnson County earthquakes exhibit spatiotemporal characteristics of seismicity induced via fluid injection processes (Davis & Frohlich, 1993; Ellsworth, 2013; Ellsworth et al., 2015; Frohlich et al., 2016). Specifically, (1) the events occur within 6 km of five SWD wells that have been operating over the time period of interest (Figure 4); (2) the hypocenters occur within shallow basement rocks along the WVF that extends through the injection unit (Figure 5); and (3) the WVF is favorably oriented for normal faulting within the modern stress regime (Lund Snee & Zoback, 2016) (Figure 5). The discussion below focuses on understanding the physical processes linking wastewater injection activity to earthquakes in northeast Johnson County over the last decade in order to examine the evolution of seismicity rates and magnitudes over the history of the reactivated fault.

The DD catalog images seismicity along the portion of the WVF that strikes NE-SW and dips to the NW (Figure 4). Focal mechanisms are consistent with normal faulting. The hypocenters occur at depths within 0.5 km of the injection unit. Temporally, the seismicity in northeast Johnson County has evolved with increasing magnitude over time (Figures 3 and S8). The M_W 4.0 earthquake, the largest earthquake of the sequence to date, occurred 7 years after the onset of injection (Figure 3), 3 years after pre-2017 peak injection volumes were reached, but on trend with a linear relationship between magnitude and the logarithm of cumulative injected volume (Figure S8). The WVF is a normal fault rooted within basement rocks that has been generating seismicity where it is favorably oriented for failure in the modern stress field, based on the orientation of $S_{H\max}$ and focal mechanism B axes. Where the fault turns away from $S_{H\max}$, we have not recorded earthquakes. The fault has exhibited minimal deformation (Figure 5) throughout geologic time (Magnani et al., 2015) but extends through the disposal formation, and likely allows the disposal formation to be in hydraulic communication with the basement, as near-critically stressed faults typically have high permeability (Zoback & Townend, 2001).

The WVF seismicity evolved similarly to other fluid injection-induced earthquake sequences in the central and eastern United States over the past decade. Like other induced sequences (Block et al., 2014;

Frohlich et al., 2014; Healy et al., 1968; Holtkamp et al., 2015; Horton, 2012; Keranen et al., 2013; Kim, 2013; Ogwari et al., 2016; Rubinstein et al., 2014; Walter et al., 2016; Yeck et al., 2015, 2017; Yeck, Weingarten, et al., 2016; Yeck, Sheehan, et al., 2016), WVF earthquakes have hypocenters in close proximity to active injection wells and the earthquakes increase in maximum magnitude with time. In Oklahoma, large-magnitude earthquakes occurred 17 years after the onset of injection (Keranen et al., 2013), at Rocky Mountain Arsenal, CO, the largest events occurred after injection activity ceased (Healy et al., 1968), and at Paradox Valley, CO, the largest earthquake to date occurred 7 years after injection operations began (Block et al., 2014; Yeck et al., 2015). Venus seismicity behaved qualitatively in a similar manner (Figure 3). Several studies outside our study region have shown a correlation between proximity of wastewater injection formation to the basement rocks, and earthquakes occurring in the crystalline basement (Holtkamp et al., 2015; Weingarten et al., 2015). This seems to be the case in the FWB (Frohlich, 2012; Frohlich et al., 2011, 2016; Hornbach et al., 2015, 2016; Justinic et al., 2013) and in Oklahoma (Walsh & Zoback, 2015). In our interpretation, seismic reflection data show the WVF and the EVF to offset the basement rocks and the Ellenburger Group, likely providing hydraulic connectivity between the injection unit and the basement rocks where seismicity develops.

The limited fault deformation associated with the WVF from the basement through the injection layer associated with the WVF is similar to seismically active regions in Colorado where active-source data are available (Block et al., 2014; Healy et al., 1968). Many faults associated with induced earthquakes display either strike-slip (e.g., McNamara, Benz, et al., 2015; McNamara, Hayes, et al., 2015) or normal (e.g., Hornbach et al., 2015) displacements and are generally consistent with published stress maps for the regions (Alt & Zoback, 2017; Lund Snee & Zoback, 2016).

It is important to note that earthquake sequences within the same sedimentary basin will not necessarily behave similarly. Within the FWB, seismicity in Venus, TX (the present study), and in Azle, TX (Hornbach et al., 2015) has been interpreted as induced. The two SWD wells associated with the Azle sequence began operations in June 2009 and December 2010 and have injected a total of 5,266,687 m^3 with an average injection pressure of ~4 MPa until September 2016. Separated by ~60 km, the seismicity in Azle and Venus occurs on previously inactive host faults that are favorably oriented for failure with respect to the modern stress regime and that crosscut the basement and overlying disposal layer. However, the seismicity has evolved differently in the two areas. First, Azle does not follow the same temporal distribution of magnitudes as Venus. The sequence began abruptly in November 2013 with a series of *M*3 earthquakes (with the largest being two M_L 3.6 earthquakes) and the seismicity rate increased rapidly from January to April 2014 (Hornbach et al., 2015). Additionally, the Azle sequence exhibited periods of swarm-like activity (>100 earthquakes in a single day), largely limited to failure within the Ellenburger. Like the earthquakes, injection data in the two areas differ. Downhole pressures and volumes in northeast Johnson County are higher than reported for wells near Azle. Taken together, the two regions suggest that the higher the fluid volume and pressure put into the system, the higher the energy release (larger magnitude earthquakes). Variations in earthquake sequence evolution within the same geologic framework emphasize the importance of studying individual sequences to better understand the underlying physical mechanisms leading to induced earthquakes.

Based on the distribution of hypocenters recorded since May 2015, the seismogenic WVF extends 5 km by 2 km, resulting in a fault area of 10 km^2. Empirical source-scaling relationships (Wells & Coppersmith, 1994) indicate that the fault could generate a *M*5.0 earthquake if it ruptured in one event, ~10 times larger than the May 2015 earthquake. Fault dimensions extracted from the seismic reflection data (Figure 5) and integrated with the hypocentral locations (Figure 4) define a fault area of at least 24.7 km^2 (3.8 km width × 6.5 km length), indicating a potential for a *M*5.4 or greater earthquake associated with the imaged WVF, if it were to rupture in a single event.

McGarr (2014) noted a general trend for induced earthquake magnitude to increase with the log of cumulative injected volume. We see a similar relationship for seismicity along the WVF (Figure S8). Yeck et al. (2015) used the upper extent of the 95% prediction interval on the linear fit to constrain maximum magnitude for induced earthquakes in the Paradox Valley, and using a similar argument here, we would expect earthquakes in the low magnitude 5 range are possible. This estimate is consistent with the fault lengths imaged by earthquakes and reflection seismic data.

The 2016 USGS One Year Hazard Map (Petersen et al., 2016) incorporated for the first time the contribution from both induced and natural earthquakes into a short-term seismic hazard forecast for the central and eastern U.S. The model distinguishes between induced and natural seismicity, including incorporating a smaller maximum magnitude assumption for induced earthquakes (*M*6) and upweighting the importance of earthquakes recorded over the previous 2 years in the induced earthquake regions. The 2016 USGS map and subsequent updates treated all Johnson County earthquakes as induced based on the Frohlich (2012) analysis. The northeast Johnson County sequence continues to grow with small magnitude earthquakes, as recorded by SMU and TexNet through 2017 and shown for late 2016 in Figure 3. Seismicity rates and magnitudes have varied over the nearly 10 years (Figure 3), and injection activity continues in the area. Cumulative injected volume will continue to increase, and the potential for significant felt earthquakes and elevated seismic hazard remains.

6. Conclusions

On 7 May 2015 a M_w 4.0 earthquake, the highest magnitude earthquake recorded in the FWB, occurred near the town of Venus, TX, prompting the deployment of a local seismic network and reanalysis of regional passive-source and seismic reflection data. Seismicity in this region began as early as 2008, coinciding with the beginning of operations of nearby SWD wells. Earthquakes recorded by the local network occurred at depths ranging from 4 to 6 km, entirely in the upper portion of the Precambrian basement. Seismic reflection data and focal mechanisms indicate a 6.5 km-long 220°N ± 20° trending normal fault that dips 57° to the northwest. High-resolution hypocenters indicate two seismic gaps, one of which is likely associated with slip during the M_w 4.0 earthquake. Reflection seismic data image two opposing faults: the east dipping Eastern Venus fault (EVF) and the west dipping Western Venus fault (WVF). Both faults are associated with subtle deformation in the Ordovician-Lower Pennsylvanian sequences and show no resolvable offset in the post-Lower Pennsylvanian rocks. The EVF and WVF strike NE-SW and are optimally oriented for failure in the modern stress field, although only the WVF is currently seismically active. Injection falloff tests conducted in May 2015 on the nearest five SWD wells indicate an overpressured disposal formation (Ellenburger Limestone) that is 0.9–4.8 MPa above hydrostatic, consistent with independent model predictions (Gono et al., 2015).

We therefore conclude that seismicity in northeast Johnson County is likely induced by the reactivation of a preexisting basement fault due to pressure perturbations caused by nearby wastewater injection operations. The near decade-long earthquake sequence exhibits characteristics typically associated with induced seismicity and occurs in a basin with intense oil and gas activity that has previously been linked to induced earthquakes (Frohlich, 2012; Frohlich et al., 2011, 2016; Hornbach et al., 2015, 2016; Justinic et al., 2013; Weingarten et al., 2015). Earthquake activity in the FWB is currently being monitored, and studies on induced seismicity in the region are ongoing. The availability of more detailed injection volume data, injection pressure data, and in situ reservoir parameters in Texas, such as has been made available in Oklahoma, would contribute significantly to the understanding of the detailed physical mechanisms leading to induced earthquakes.

The study has significant implications for seismic hazard assessment in North Texas and other regions of anthropogenic seismicity. We document substantial evidence for the anthropogenic character of the 2015 M_w 4.0 earthquake and related seismicity over the last decade and provide improved estimates of fault areas and geometries. The WVF seismogenic area scales to a middle magnitude 5, which is not inconsistent with induced earthquakes documented in Oklahoma (Keranen et al., 2013; Yeck et al., 2017; Yeck, Weingarten, et al., 2016). Additionally, we show that North Texas faults can generate earthquakes on a long time scale under continuous SWD operations and that magnitude increases with time and cumulative injected volume on the WVF. Since SWD operations continue in northeast Johnson County, the 2015 M_w 4.0 may be neither the final nor largest earthquake in this sequence.

Acknowledgments

We thank Matthew Weingarten, William Stephenson, Julie Herrick, and an anonymous reviewer for comments that improved the manuscript. We additionally thank Brian Stump, Chris Hayward, and Cliff Frohlich for insightful comments on initial drafts; SMU students Kevin Kwong Harrison Oldham and Elizabeth Layton for their aid with this project; IRIS interns Mason Phillips and Shawn Lee for their work on improving processing techniques. The study was partially supported by the U.S. Geological Survey Earthquake Hazard Program (G15AC00141 and G16AC00247 to HRD and MBM), and IRIS. Internal financial support from the SMU Research Council, SMU Huffington Department of Earth Sciences, Institute for the Study of Earth and Man at SMU, and Univ. of Texas Institute for Geophysics facilitated network operations. Figures were made using Generic Mapping Tool (Wessel & Smith, 1998). Supporting data are archived as described in the text or can be found in the supporting information. We thank Seismic Exchange, Inc. for permission to display the seismic reflection data. Any use of trade, firm, or product names is for descriptive purposes only and does not imply endorsement by the U.S. Government.

References

Alt, R. C., & Zoback, M. D. (2017). *In situ* stress and active faulting in Oklahoma. *Bulletin of the Seismological Society of America*, *107*(1). https://doi.org/10.1785/0120160156

Beroza, G. C., & Zoback, M. D. (1993). Mechanism diversity of the Loma Prieta aftershocks and the mechanics of mainshock-aftershock interaction. *Science*, *259*(5092), 210–213.

Block, L. V., Wood, C. K., Yeck, W. L., & King, V. M. (2014). The 24 January 2013 M_L 4.4 earthquake near Paradox, Colorado, and its relation to deep well injection. *Seismological Research Letters*, *85*(3), 609–624. https://doi.org/10.1785/0220130188

Davis, S. D., & Frohlich, C. (1993). Did (or will) fluid injection cause earthquakes?—Criteria for rational assessment. *Seismological Research Letters*, *64*(3–4), 207–224. https://doi.org/10.1785/gssrl.64.3-4.207

DeShon, H. R., & Magnani, M. B. (2016). Final technical report for G15AC00141: North Texas earthquake studies and network operations, submitted to the United States Geological Survey, October 4, 2016.

Ellsworth, W. L. (2013). Injection-induced earthquakes. *Science*, *341*(6142), 1225942. https://doi.org/10.1126/science.1225942

Ellsworth, W. L., Llenos, A. L., McGarr, A. F., Michael, A. J., Rubinstein, J. L., Mueller, C. S., … Calais, E. (2015). Increasing seismicity in the US midcontinent: Implications for earthquake hazard. *The Leading Edge*, *34*(6), 618–626. https://doi.org/10.1190/tle34060618.1

Ewing, T. E., Budnik, R. T., Ames, J. T., Ridner, D. M., & Dillon, R. (1990). *Tectonic map of Texas, Bureau of Economic Geology*. Austin, TX: The Univ. of Texas.

Fan, Z., Eichhubl, P., & Gale, J. F. (2016). Geomechanical analysis of fluid injection and seismic fault slip for the M_w4. 8 Timpson, Texas, earthquake sequence. *Journal of Geophysical Research: Solid Earth*, *121*, 2798–2812. https://doi.org/10.1002/2016JB012821

Frohlich, C. (2012). Two-year survey comparing earthquake activity and injection-well locations in the Barnett Shale, Texas. *Proceedings of the National Academy of Sciences of the United States of America*, *109*(35), 13,934–13,938. https://doi.org/10.1073/pnas.1207728109

Frohlich, C., DeShon, H., Stump, B., Hayward, C., Hornbach, M., & Walter, J. I. (2016). A historical review of induced earthquakes in Texas. *Seismological Research Letters*, *87*(4), 1022–1038. https://doi.org/10.1785/0220160016

Frohlich, C., Ellsworth, W., Brown, W. A., Brunt, M., Luetgert, J., MacDonald, T., & Walter, S. (2014). The 17 May 2012 *M*4.8 earthquake near Timpson, East Texas: An event possibly triggered by fluid injection. *Journal of Geophysical Research: Solid Earth*, *119*, 581–593. https://doi.org/10.1002/2013JB010755

Frohlich, C., Hayward, C., Stump, B., & Potter, E. (2011). The Dallas-Fort Worth earthquake sequence: October 2008 through May 2009. *Bulletin of the Seismological Society of America*, *101*(1), 327–340. https://doi.org/10.1785/0120100131

Gono, V., Olson, J. E., & Gale, J. F. (2015). Understanding the correlation between induced seismicity and wastewater injection in the Fort Worth Basin, Paper presented at *49th US Rock Mechanics/Geomechanics Symposium*, American Rock Mechanics Association.

Hardebeck, J. L., & Shearer, P. M. (2002). A new method for determining first-motion focal mechanisms. *Bulletin of the Seismological Society of America*, *92*(6), 2264–2276. https://doi.org/10.1785/0120010200

Hardebeck, J. L., & Shearer, P. M. (2003). Using *S/P* amplitude ratios to constrain the focal mechanisms of small earthquakes. *Bulletin of the Seismological Society of America*, *93*(6), 2434–2444. https://doi.org/10.1785/0120020236

Healy, J. H., Rubey, W. W., Griggs, D. T., & Raleigh, C. B. (1968). The Denver earthquakes. *Science*, *161*(3848), 1301–1310. https://doi.org/10.1029/WR026i007p01631

Herrmann, R. B. (2013). Computer programs in seismology: An evolving tool for instruction and research. *Seismological Research Letters*, *84*(6), 1081–1088. https://doi.org/10.1785/0220110096

Holtkamp, S. G., Brudzinski, M. R., & Currie, B. S. (2015). Regional detection and monitoring of injection-induced seismicity: Application to the 2010–2012 Youngstown, Ohio, seismic sequence. *AAPG Bulletin*, *99*(9), 1671–1688. https://doi.org/10.1306/03311513194

Hornbach, M. J., DeShon, H. R., Ellsworth, W. L., Stump, B. W., Hayward, C., Frohlich, C., … Luetgert, J. H. (2015). Causal factors for seismicity near Azle, Texas. *Nature Communications*, *6*, 11. https://doi.org/10.1038/ncomms7728

Hornbach, M. J., Jones, M., Scales, M., DeShon, H. R., Magnani, M. B., Frohlich, C., … Layton, M. (2016). Ellenburger wastewater injection and seismicity in North Texas. *Physics of the Earth and Planetary Interiors*, *261*, 54–68. https://doi.org/10.1016/j.pepi.2016.06.012

Horton, S. (2012). Disposal of hydrofracking waste fluid by injection into subsurface aquifers triggers earthquake swarm in central Arkansas with potential for damaging earthquake. *Seismological Research Letters*, *83*(2), 250–260. https://doi.org/10.1785/gssrl.83.2.250

Janská, E., & Eisner, L. (2012). Ongoing seismicity in the Dallas-Fort Worth area. *The Leading Edge*, *31*(12), 1462–1468. https://doi.org/10.1190/tle31121462

Justinic, A. H., Stump, B., Hayward, C., & Frohlich, C. (2013). Analysis of the Cleburne, Texas, earthquake sequence from June 2009 to June 2010. *Bulletin of the Seismological Society of America*, *103*(6), 3083–3093. https://doi.org/10.1785/0120120336

Kato, A., Obara, K., Igarashi, T., Tsuruoka, H., Nakagawa, S., & Hirata, N. (2012). Propagation of slow slip leading up to the 2011 M_w 9.0 Tohoku-Oki earthquake. *Science*, *335*(6069), 705–708. https://doi.org/10.1126/science.1215141

Keranen, K. M., Savage, H. M., Abers, G. A., & Cochran, E. S. (2013). Potentially induced earthquakes in Oklahoma, USA: Links between wastewater injection and the 2011 M_w 5.7 earthquake sequence. *Geology*, *41*(6), 699–702. https://doi.org/10.1130/G34045.1

Kier, R. S. (1988). The Precambrian of central Texas. In O. T. Hayward (Ed.), *South-central section, geological society of America centennial field guide* (Vol. 4, pp. 351–360). Boulder, CO: Geological Society of America.

Kim, W. Y. (2013). Induced seismicity associated with fluid injection into a deep well in Youngstown, Ohio. *Journal of Geophysical Research: Solid Earth*, *118*, 3506–3518. https://doi.org/10.1002/jgrb.50247

Lund Snee, J. E., & Zoback, M. D. (2016). State of stress in Texas: Implications for induced seismicity. *Geophysical Research Letters*, *43*, 10,208–10,214. https://doi.org/10.1002/2016GL070974

Magnani, M. B., Hornbach, M. J., DeShon, H. R., Hayward, C., & Blanpied, M. L. (2015). *Discriminating between induced vs. tectonic seismicity from long-term history of fault behavior in intraplate regions*. Abstract S11C-01 presented at the 2015 Fall Meeting, AGU, San Francisco, CA. 14–18 December.

McGarr, A. (2014). Maximum magnitude earthquakes induced by fluid injection. *Journal of Geophysical Research: Solid Earth*, *119*, 1008–1019. https://doi.org/10.1002/2013JB010597

McNamara, D. E., Benz, H. M., Herrmann, R. B., Bergman, E. A., Earle, P., Holland, A., … Gassner, A. (2015). Earthquake hypocenters and focal mechanisms in central Oklahoma reveal a complex system of reactivated subsurface strike-slip faulting. *Geophysical Research Letters*, *42*, 2742–2749. https://doi.org/10.1002/2014GL062730

McNamara, D. E., Hayes, G. P., Benz, H. M., Williams, R. A., McMahon, N. D., Aster, R. C., … Earle, P. (2015). Reactivated faulting near Cushing, Oklahoma: Increased potential for a triggered earthquake in an area of United States strategic infrastructure. *Geophysical Research Letters*, *42*, 8328–8332. https://doi.org/10/1002/2015GL064669

Meng, X., Peng, Z., & Hardebeck, J. L. (2013). Seismicity around Parkfield correlates with static shear stress changes following the 2003 M_w 6.5 San Simeon earthquake. *Journal of Geophysical Research: Solid Earth*, *118*, 3576–3591. https://doi.org/10.1002/jgrb.50271

Nicot, J. P., Scanlon, B. R., Reedy, R. C., & Costley, R. A. (2014). Source and fate of hydraulic fracturing water in the Barnett Shale: A historical perspective. *Environmental Science and Technology*, *48*(4), 2464–2471.

Ogwari, P. O., Horton, S. P., & Ausbrooks, S. (2016). Characteristics of induced/triggered earthquakes during the startup phase of the Guy–Greenbrier earthquake sequence in North–Central Arkansas. *Seismological Research Letters*, *87*(3), 620–630. https://doi.org/10.1785/0220150252

Pavlis, G. L., Vernon, F., Harvey, D., & Quinlan, D. (2004). The generalized earthquake-location (GENLOC) package: An earthquake-location library. *Computers and Geosciences*, *30*(9), 1079–1091. https://doi.org/10.1016/j.cageo.2004.06.010

Petersen, M. D., Mueller, C. S., Moschetti, M. P., Hoover, S. M., Llenos, A. L., Ellsworth, W. L., ... Rukstales, K. S. (2016). 2016 one-year seismic hazard forecast for the Central and Eastern United States from induced and natural earthquakes (No. 2016-1035). US Geological Survey. https://doi.org/10.3133/ofr20161035

Pollastro, R. M., Jarvie, D. M., Hill, R. J., & Adams, C. W. (2007). Geologic framework of the Mississippian Barnett Shale, Barnett-Paleozoic total petroleum system, Bend Arch-Fort Worth Basin, Texas. *AAPG Bulletin*, *91*(4), 405–436. https://doi.org/10.1306/1030606008

Reiter, D., Leidig, M., Yoo, S.-Y., & Mayeda, K. (2012). Source characteristics of seismicity associated with underground wastewater disposal: A case study from the 2008 Dallas-Fort Worth earthquake sequence. *The Leading Edge*, *31*(12), 1454–1460. https://doi.org/10.1190/tle31121454

Reyes, C. G., & West, M. E. (2011). The waveform suite: A robust platform for manipulating waveforms in MATLAB. *Seismological Research Letters*, *82*(1), 105–110. https://doi.org/10.1785/gssrl.82.1.104

Rubinstein, J. L., Ellsworth, W. L., McGarr, A., & Benz, H. M. (2014). The 2001–present induced earthquake sequence in the Raton Basin of northern New Mexico and southern Colorado. *Bulletin of the Seismological Society of America*, *104*(5), 2162–2181. https://doi.org/10.1785/0120140009

Rubinstein, J. L., & Mahani, A. B. (2015). Myths and facts on wastewater injection, hydraulic fracturing, enhanced oil recovery, and induced seismicity. *Seismological Research Letters*, *86*(4), 1–8. https://doi.org/10.1785/0220150067

Scales, M. (2017). A decade of induced slip on the causative fault of the 2015 MW 4.0 Venus earthquake (Master's thesis, Southern Methodist University). Retrieved from https://search.proquest.com/docview/1916810295

Shen, Y., Forsyth, D. W., Conder, J., & Dorman, L. M. (1997). Investigation of microearthquake activity following an intraplate teleseismic swarm on the west flank of the southern East Pacific Rise. *Journal of Geophysical Research*, *102*(B1), 459–475. https://doi.org/10.1029/96JB02852

Skoumal, R. J., Brudzinski, M. R., Currie, B. S., & Levy, J. (2014). Optimizing multi-station earthquake template matching through re-examination of the Youngstown, Ohio, sequence. *Earth and Planetary Science Letters*, *405*, 274–280. https://doi.org/10.1016/j.epsl.2014.08.033

Sullivan, E. C., Marfurt, K. J., Lacazette, A., & Ammerman, M. (2006). Application of new seismic attributes to collapse chimneys in the Fort Worth Basin. *Geophysics*, *71*(4), B111–B119. https://doi.org/10.1190/1.2216189

Thomas, W. A. (2006). Tectonic inheritance at a continental margin. *GSA Today*, *16*(2), 4–11.

Thomas, W. A. (2011). Detrital-zircon geochronology and sedimentary provenance. *Lithosphere*, *3*(4), 304–308. https://doi.org/10.1130/RF.L001.1

Thomas, W. A., Viele, G. W., Arbenz, J. K., Nicholas, R. L., Denison, R. E., Muehlberger, W. R., & Tauvers, P. R. (1989). Tectonic map of the Ouachita orogen, and cross sections of the Appalachian-Ouachita orogen beneath the Gulf Coastal Palin. *The Appalachian-Ouachita Orogen in the United States*, *Geol. of North Am*, *2*, 9.

Waldhauser, F., & Ellsworth, W. L. (2000). A double-difference earthquake location algorithm: Method and application to the northern Hayward fault, California. *Bulletin of the Seismological Society of America*, *90*(6), 1353–1368. https://doi.org/10.1785/0120000006

Walsh, F. R., & Zoback, M. D. (2015). Oklahoma's recent earthquakes and saltwater disposal. *Science Advances*, *1*(5), e1500195. https://doi.org/10.1126/sciadv.1500195

Walter, J. I., Dotray, P. J., Frohlich, C., & Gale, J. F. (2016). Earthquakes in northwest Louisiana and the Texas–Louisiana border possibly induced by energy resource activities within the Haynesville Shale Play. *Seismological Research Letters*, *87*(2A). https://doi.org/10.1785/0220150193

Walter, J. I., Meng, X., Peng, Z., Schwartz, S. Y., Newman, A. V., & Protti, M. (2015). Far-field triggering of foreshocks near the nucleation zone of the 5 September 2012 (M_W 7.6) Nicoya Peninsula, Costa Rica earthquake. *Earth and Planetary Science Letters*, *431*, 75–86. https://doi.org/10.1016/j.epsl.2015.09.017

Weingarten, M., Ge, S., Godt, J. W., Bekins, B. A., & Rubinstein, J. L. (2015). High-rate injection is associated with the increase in US mid-continent seismicity. *Science*, *348*(6241), 1336–1340. https://doi.org/10.1126/science.aab1345

Wells, D. L., & Coppersmith, K. J. (1994). New empirical relationships among magnitude, rupture length, rupture width, rupture area, and surface displacement. *Bulletin of the Seismological Society of America*, *84*(4), 974–1002.

Wessel, P., & Smith, W. H. (1998). New, improved version of Generic Mapping Tools released. *Eos*, *79*(47), 579–579. https://doi.org/10.1029/98EO00426

Yeck, W. L., Block, L. V., Wood, C. K., & King, V. M. (2015). Maximum magnitude estimations of induced earthquakes at Paradox Valley, Colorado, from cumulative injection volume and geometry of seismicity clusters. *Geophysical Journal International*, *200*(1), 322–336. https://doi.org/10.1002/2013JB0101597

Yeck, W. L., Hayes, G. P., McNamara, D. E., Rubinstein, J. L., Barnhart, W. D., Earle, P. S., & Benz, H. M. (2017). Oklahoma experiences largest earthquake during ongoing regional wastewater injection hazard mitigation efforts. *Geophysical Research Letters*, *44*, 711–717. https://doi.org/10.1002/2016GL071685

Yeck, W. L., Sheehan, A. F., Benz, H. M., Weingarten, M., & Nakai, J. (2016). Rapid response, monitoring, and mitigation of induced seismicity near Greeley, Colorado. *Seismological Research Letters*, *87*(4), 837–847. https://doi.org/10.1785/0220150275

Yeck, W. L., Weingarten, M., Benz, H. M., McNamara, D. E., Bergman, E. A., Herrmann, R. B., … Earle, P. S. (2016). Far-field pressurization likely caused one of the largest injection induced earthquakes by reactivating a large preexisting basement fault structure. *Geophysical Research Letters*, *43*, 10,198–10,207. https://doi.org/10.1002/2016GL070861

Zhang, H., & Thurber, C. H. (2003). Double-difference tomography: The method and its application to the Hayward Fault, California. *Bulletin of the Seismological Society of America*, *93*(5), 1875–1889. https://doi.org/10.1785/0120020190

Zoback, M. D., & Townend, J. (2001). Implications of hydrostatic pore pressures and high crustal strength for the deformation of intraplate lithosphere. *Tectonophysics*, *336*(1), 19–30. https://doi.org/10.1016/S0040-1951(01)00091-9